Cable-less, Magnetically-Driven Forceps For Minimally Invasive Surgery

Cameron Forbrigger, Andrew Lim, Onaizah Onaizah, Sajad Salmanipour, Thomas Looi, James Drake, and Eric Diller*

***Abstract*—A novel end-effector for surgical applications is presented that uses magnetic actuation in lieu of a more traditional cable-driven tool with the goal of providing high dexterity in hard-to-reach locations by decoupling the tool actuation from the rest of the surgical system. The gripper and wrist device consists of several magnets connected with compliant Nitinol joints that allow two rotational degrees of freedom and one gripping degree of freedom. As an end effector for an existing surgical robot arm, this device could augment existing minimally invasive surgical robots by allowing high distal dexterity in surgical sites with narrow and restricted access. A static deflection model of the device is used to design an open loop controller. The current prototype is capable of exerting pushing/pulling forces of 9 mN and gripping forces of 6 mN when magnetic flux densities of 20 mT are applied by a laboratory-scale electromagnetic coil system. These forces could be greatly amplified in a clinical-scale system to make brain tissue resection feasible. Under open loop control, the wrist of the device can maneuver from $+\pi/4$ rad to $-\pi/4$ rad in less than one second with a maximum error of 0.12 rad.**

***Index Terms*—Grippers and Other End-Effectors, Surgical Robotics: Laparoscopy, Micro/Nano Robots**

I. Introduction

ROBOT-assisted minimally invasive approaches are used in gynecology, urology, orthopedic surgery, gastroenterology, and general surgery [1]. Commercially available platforms, such as the Da Vinci Surgical System from Intuitive Surgical [2], are seeing increased adoption in a variety of procedures. However, robot-assisted minimally invasive surgical (MIS) approaches remain largely absent in surgical disciplines with much narrower workspaces, such as neurosurgery or pediatric cases [3], [4]. In the field of endoscopic neurosurgery, there is an overall lack of effective complementary tools, such as bipolar forceps, thus limiting robotic approaches [5].

Endoscopic resection of intraventricular brain tumors is becoming more common, but the operability of certain tumors is limited by the size of the ventricles of the patient and the location of the tumor [6]. Smaller tools with higher dexterity would improve the range of operable intraventricular tumors, especially in pediatric procedures.

With the exception of multi-backbone continuum robots, existing robotic MIS approaches contain moving parts with sliding contacts. Frictional losses become more significant with greater miniaturization, and they can affect the accuracy and repeatability of these robots. Moreover, existing MIS robots experience a trade-off between the ability to navigate several tools to the surgical site and the distal dexterity of the tools upon reaching the site. Cable-drives are a common method of tool actuation, but significant physical challenges hinder further miniaturization. Smaller tools require smaller diameter pulleys, thereby reducing the mechanical advantage and increasing the required cable tension. Smaller cable diameters would also be necessary, thereby reducing the allowable tension. Combined with increased frictional effects on smaller scales, these factors increase the likelihood of cable failure in these tools [7]. Improving the material strength and friction properties has allowed the creation of tools as small as 3 mm (Medical Micro Instruments, Pisa, Italy), but further miniaturization may require alternative actuation methods.

Wireless magnetic actuation may be feasible for augmenting existing MIS robots. Magnetically-actuated microrobots are capable of high-precision tissue penetration [8] and sub-millimeter manipulation tasks [9]. Magnetic steering has been implemented for catheters [10], endoscopes [11], and micro grippers [12]. Uniform magnetic fields can be used to control up to eight independent degrees of freedom [13], which can allow multiple simple mechanisms, or a single complex mechanism, to be controlled within the same workspace. High-power, clinical-scale electromagnetic coil systems are being developed that are capable of precise control of magnetic fields with workspaces the size of an adult torso and maximum flux densities up to 400 mT [14].

A magnetically-actuated end effector mounted at the distal end of an existing surgical robot arm could increase the distal dexterity of the robot without reducing its narrow access navigation capabilities. In addition, the wireless, cable-less nature of the end effector could allow for greater miniaturization of the robot arm because the arm would not need to accommodate any mechanical or electrical transmission to power the end effector. Furthermore, the tool could allow for a modular design that can be attached to the distal end of many different types of robot arms.

In this work, we explore the modeling and feasibility of a

Manuscript received: Sept. 9, 2018; Revised Dec. 1, 2018; Accepted Jan. 3, 2019.

This paper was recommended for publication by Editor P. Valdastri upon evaluation of the Reviewers' comments. This work was supported by the Natural Sciences and Engineering Research Council of Canada through the Discovery Grant Program 2014-04703, by the Ontario Student Opportunity Trust Fund (OSOTF), and by Toronto SickKids Restracomp.

*Corresponding author.

C. Forbrigger, O. Onaizah, S. Salmanipour, and E. Diller are with the Department of Mechanical and Industrial Engineering, University of Toronto, Toronto, ON Canada ediller@mie.utoronto.ca

A. Lim is with the Institute of Biomaterials and Biomedical Engineering, University of Toronto, Toronto, ON Canada

A. Lim, T. Looi, and J. Drake are with the Centre for Image Guided Innovation and Therapeutic Intervention (CIGITI), Toronto Hospital for Sick Children, Toronto, ON Canada

Digital Object Identifier (DOI): see top of this page.

This article has been accepted for publication in a future issue of this journal, but has not been fully edited. Content may change prior to final publication. Citation information: DOI 10.1109/LRA.2019.2894504, IEEE Robotics and Automation Letters

cable-less, magnetically-actuated, 3-degree-of-freedom (DOF) gripper prototype. Fig. 1 shows the gripper prototype. This device can fit through a 4 mm diameter hole. We show that the gripper can be accurately controlled with an open loop control scheme. Furthermore, we demonstrate the feasibility of the gripper for use in surgical procedures by measuring the forces that the gripper is capable of applying.

II. Fabrication and Modeling

The device is a fully-compliant mechanism, that is, connections between the components are made with flexible beams instead of revolute joints, thereby reducing friction and improving positional repeatability. The finger joints and 2-DOF wrist are composed of superelastic Nitinol wires. The other components of the frame are composed of titanium. Three neodymium iron boride N52 grade magnets are attached to the titanium frame: one for the wrist and one for each finger. The placement and magnetization directions of the magnets are shown in Fig. 1(b). The gripper digits, flexure joints, and permanent magnets were prepared individually and joined using a LaserStar iWeld 990 series laser welder. The curved geometry of the finger flexure joints was achieved by shape setting the Nitinol wire in a custom high-temperature jig at 550 °C. The length of the gripper, including the wrist flexure joint, is 21 mm.

A. Operating Principle

Fig. 2 shows the operating principle of the magnetic gripper. By applying a uniform magnetic field to the gripper, a total of three degrees of freedom can be independently controlled: two rotational degrees of freedom in the wrist and one degree of freedom opening and closing the fingers. If the field has only a component perpendicular $\mathbf{B}_\perp$ to the wrist magnetic moment $\mathbf{m}_w$, the gripper wrist will rotate without closing the fingers. Figure 2 shows in-plane rotation, but the wrist can also rotate out of plane. A field with only a component parallel $\mathbf{B}_\parallel$ to $\mathbf{m}_w$ will cause the fingers to close without the wrist rotating. If a field $\mathbf{B}$ is applied to the gripper with components both perpendicular and parallel to $\mathbf{m}_w$, the gripper will both turn and close.

An analytical model of the gripper is needed to determine the required magnetic field direction and magnitude to reach a desired gripper pose. This model will be necessary for the open loop control scheme that is presented later in the paper.

B. Gripper Model

This section describes the methods used to model the deflections of the gripper when subjected to known magnetic inputs. The present model assumes static deflections from the resting position of the beam and relatively small cargo weights compared to the magnetic torques so that the resting orientation can be approximated as the x-axis. Carrying cargo will change the resting orientation of the beam in the vertical direction depending on the weight of the load, but if the beam deflection remains in the elastic region this model remains valid from the new resting orientation. Accounting for the dynamics of the gripper will be an area of future work.

The torque due to the static elastic deformation of a cantilever beam is proportional to the included angle θ between the tangent vector to the free end of the beam and its zero-deformation orientation, as shown in Fig. 2(b). The direction of the elastic torque on the wrist is normal to the plane formed by the relaxed orientation of the wrist $\hat{\mathbf{i}}$ and the orientation of

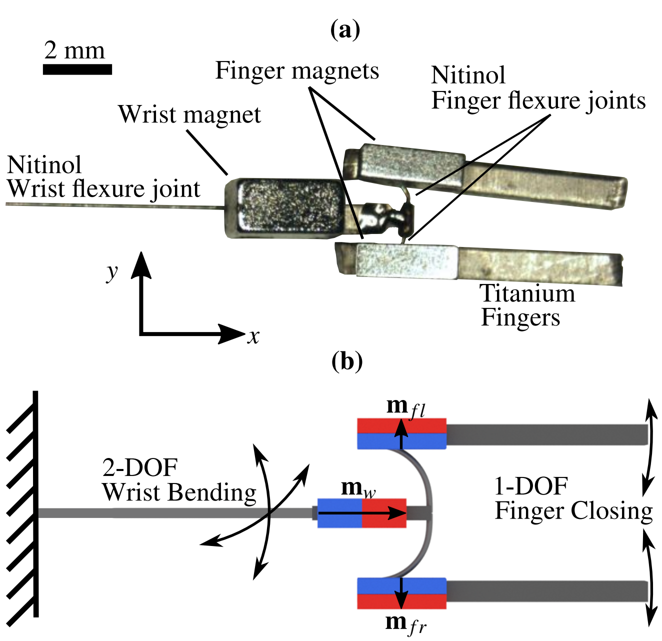

Fig. 1. (a) Photograph of the gripper. (b) Gripper schematic (not to scale) showing magnet locations and magnetization directions.

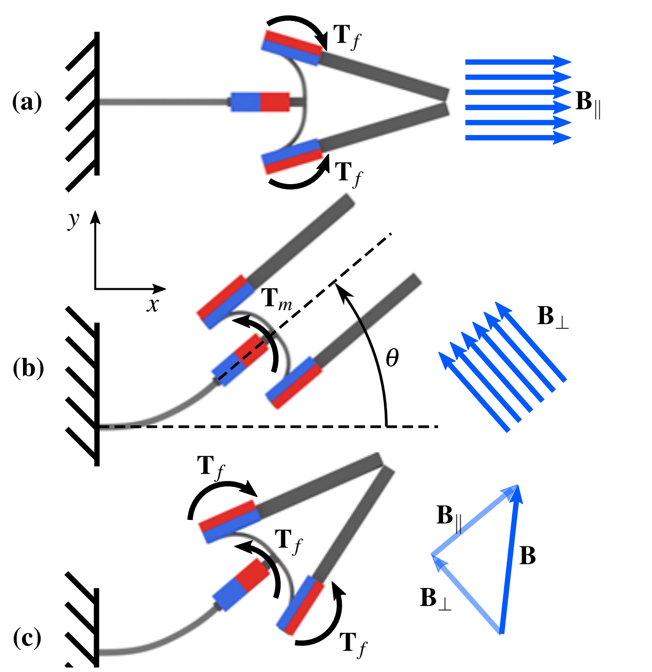

Fig. 2. Gripper operating principle. **(a)** A parallel field closes the gripper fingers, **(b)** a perpendicular field turns the gripper wrist, **(c)** combining both parallel and perpendicular fields both turns the wrist and closes the fingers.

the wrist $\mathbf{m}_w$. The elastic torque acts in the negative direction for positive theta, that is,

$$\mathbf{T}_k = -k\theta \left(\frac{\hat{\mathbf{i}} \times \mathbf{m}_w}{\|\hat{\mathbf{i}} \times \mathbf{m}_w\|} \right). \tag{1}$$

where k is the angular stiffness of the wrist. For a cantilever beam with constant cross-section and material properties in the linear elastic range the angular stiffness is $k = EI/L$, where E is the elastic modulus, I is the area moment of inertia, and L is the length of the beam.

The wrist magnet of the gripper is rigidly attached to the free end of a Nitinol beam with its magnetic dipole moment vector $\mathbf{m}_w$ tangent to the free end of the beam, as shown in Fig. 1(b). Let the zero-deformation orientation of the free end of the beam be $\hat{\mathbf{i}}$, the x-direction unit vector. The angle θ between $\mathbf{m}_w$ and its zero-deformation orientation $\hat{\mathbf{i}}$ is

$$\tan\theta = \frac{\|\hat{\mathbf{i}} \times \mathbf{m}_w\|}{\hat{\mathbf{i}} \cdot \mathbf{m}_w}. \tag{2}$$

The vector $\mathbf{B}$ describes a uniform magnetic flux density applied throughout the workspace of the gripper. This vector can be represented as the sum of components normal $\mathbf{B}_\perp$ and parallel $\mathbf{B}_\parallel$ to $\mathbf{m}_w$, that is,

$$\mathbf{B} = \mathbf{B}_\perp + \mathbf{B}_\parallel. \tag{3}$$

The magnetic torque applied to $\mathbf{m}_w$ by $\mathbf{B}$ is

$$\mathbf{T}_m = \mathbf{m}_w \times \mathbf{B} = \mathbf{m}_w \times \mathbf{B}_\perp. \tag{4}$$

$\mathbf{B}_\parallel$ does not contribute to the magnetic torque applied to the wrist because $\mathbf{m}_w \times \mathbf{B}_\parallel = 0$.

At the equilibrium position for a given applied magnetic field, the sum of the torques must be zero ($\mathbf{T}_m = -\mathbf{T}_k$). The $\mathbf{B}_\perp$ necessary to achieve a given value of θ can be determined by substituting (1) and (4) and solving for $\mathbf{B}_\perp$, which yields

$$\mathbf{B}_\perp = \frac{k\theta}{m_w} \left(\frac{\mathbf{m}_w \times \mathbf{T}_k}{\|\mathbf{m}_w \times \mathbf{T}_k\|} \right). \tag{5}$$

The magnetic field can be produced using electromagnetic (EM) coils. The relationship between the EM coil currents and the applied magnetic fields can be treated as linear within the workspace of three orthogonal pairs of Helmholtz coils:

$$\mathbf{B} = \mathbf{K}\mathbf{I}, \tag{6}$$

where $\mathbf{I}$ is a 3×1 vector of input EM coil currents to each pair of coils, and $\mathbf{K}$ is a 3×3 constant diagonal matrix.

C. Definition of the Robot Orientation

The gripper wrist is capable of rotational motion with two degrees of freedom. Fig. 3 shows the wrist magnetic moment vector $\mathbf{m}_w$ rotated by an azimuth angle $-\pi \le \gamma \le \pi$ and altitude angle $-\frac{\pi}{2} \le \beta \le \frac{\pi}{2}$. The perpendicular magnetic field vector $\mathbf{B}_\perp$, and the included angle θ between the magnetic moment $\mathbf{m}_w$ and its resting position $\hat{\mathbf{i}}$ are also shown in a rotated view of the plane defined by $\mathbf{m}_w$ and $\hat{\mathbf{i}}$.

The coils in the electromagnetic coil system are positioned along the x-, y-, and z- axes of the Cartesian coordinate system in Fig. 3. The wrist magnetic dipole moment and the parallel magnetic field component can be described in Cartesian coordinates using the azimuth and altitude angles as

$$\mathbf{m}_w = m_w \left((\cos\beta\cos\gamma)\hat{\mathbf{i}} + (\cos\beta\sin\gamma)\hat{\mathbf{j}} + (\sin\beta)\hat{\mathbf{k}} \right), \tag{7}$$

$$\mathbf{B}_\parallel = B_\parallel \left((\cos\beta\cos\gamma)\hat{\mathbf{i}} + (\cos\beta\sin\gamma)\hat{\mathbf{j}} + (\sin\beta)\hat{\mathbf{k}} \right). \tag{8}$$

For the position of the end effector, we model the gripper wrist as a spherical joint located at one third of the length of the wrist beam along the beam centerline with a rotational stiffness of k. We also assume that the gripper fingers, because of their relatively small deflections, can be modeled as revolute joints located halfway between the wrist and the fingers with rotational stiffness k_f.

In summary, θ can be calculated for a given position defined by γ and β using (7) and (2). Then, the perpendicular magnetic field vector $\mathbf{B}_\perp$ required to reach the desired pose can be calculated using (5). Finally, the gripper fingers can open and close by applying the parallel magnetic field component $\mathbf{B}_\parallel$ calculated using (8).

III. Control System

Open loop control is not capable of compensating for external loads and usually has worse performance than closed loop control. However, in MIS applications, acquiring accurate feedback, especially at high enough rates for effective closed loop control, is a significant problem. Present tools operate with the surgeon in the loop providing commands based on video feedback from an endoscope. Regardless of whether closed loop control is used, accurate knowledge of the open loop dynamics is useful for cases where feedback may be periodically or temporarily absent.

An open loop control scheme was designed to control the orientation of the gripper. The user inputs the desired azimuth γ_d and altitude β_d angles of the gripper. The control system estimates the present azimuth γ_e and altitude β_e angles of the gripper using the analytical model and the present known applied magnetic field. Using the desired and estimated poses of the gripper, the EM coil model, and the gripper model, an algorithm determines the control input to produce a piece-wise constant-jerk trajectory from $[\gamma_e, \beta_e]$ to $[\gamma_d, \beta_d]$. Then, a computer vision system measures the output gripper pose, γ_m and β_m. These pose measurements are used to measure the performance of the open loop controller. The maximum angular velocities $\dot{\gamma}_{max}$ and $\dot{\beta}_{max}$, angular accelerations $\ddot{\gamma}_{max}$

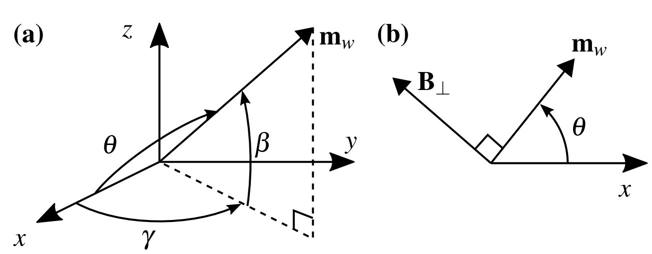

Fig. 3. **(a)** Wrist magnetic moment vector $\mathbf{m}_w$ in spherical coordinates. **(b)** Rotated view of the plane formed by $\mathbf{m}_w$ and $\hat{\mathbf{i}}$.

This article has been accepted for publication in a future issue of this journal, but has not been fully edited. Content may change prior to final publication. Citation information: DOI 10.1109/LRA.2019.2894504, IEEE Robotics and Automation Letters

and $\ddot{\beta}_{max}$, and angular jerk $\dddot{\gamma}_{max}$ and $\dddot{\beta}_{max}$ for the constant-jerk trajectory can be specified by the user.

IV. Experimental Setup

These experiments demonstrate the range of motion, accuracy, repeatability, and applied forces of the gripper.

The experimental setup used is shown in Fig. 4. An electromagnetic coil system consisting of three orthogonal Helmholtz coil pairs was used to apply uniform magnetic fields to the gripper. The coil system can produce a controlled magnetic flux density $\mathbf{B}$ in three dimensions within a workspace of 20 mm by 30 mm up to a maximum flux density of 20 mT with a cutoff frequency of 60 Hz. The current to each pair of coils is controlled by a Sensoray S826 PCI Express board. The gripper orientation was measured using video at 60 fps from two FOculus FO124TC firewire cameras viewing the xy (top view) and xz (side view) planes, respectively. The orientation of the wrist magnet was detected by the overhead camera using computer vision algorithms from OpenCV.

V. Results and Discussion

A. Model Validation

The wrist joint of the gripper should be capable of significant linear deformation and highly repeatable positioning. This experiment demonstrates the linearity, range of motion, repeatability and analytical model accuracy of the gripper.

The loading/unloading curve from $+10$ mT to $-10mT$ is shown in Fig. 5. A known perpendicular magnetic flux density $B_\perp$ was applied to the gripper in the horizontal plane and the resulting steady-state angular position of the wrist magnet was measured. Larger field magnitudes were available from the coil system, and therefore wrist deflections larger than $\pm\pi/2$ rad are possible; however, at $\theta = \pm\pi/2$ rad the wrist reaches a singularity and becomes difficult to control. Larger deflections may require more sophisticated closed loop control methods with higher-quality feedback.

From (5), the model predicts a linear relationship between $B_\perp$ and θ. Inserting the known material properties, magnetic properties and dimensions of the gripper prototype into (5) yields $k/m_w = 7.4$ mT/rad with a combined measurement uncertainty of 4%. The slope of the linear best-fit line of the experimental data shown in Fig. 5 was $k/m_w = 8.1$ mT/rad with a root mean sum of squared residuals (RMSE) of 0.11 mT. The data show excellent agreement with the proposed linear model, and there is no observable hysteresis in the loading-unloading curve. The experimental k/m_w differs from the predicted k/m_w by 10%; therefore, while the predicted k/m_w provides a reasonable model for the gripper motion, experimental model fitting significantly improves the accuracy of the static deflection model.

B. Force Measurements

The feasibility of the gripper depends on its ability to exert gripping and pushing or pulling forces on tissue. The gripper forces were measured using a single-axis GSO100 load cell (Transducer Technologies). The load cell has a rated accuracy of ± 0.8 mN. For measuring the push/pull force, the gripper fingers were held in a jig connected to the transducer of the load cell while perpendicular magnetic flux was applied to the gripper. For measuring the gripping force, the gripper wrist was held stationary and a single gripper finger was attached to a titanium wire that was rigidly connected to the transducer of the load cell while parallel magnetic flux was applied to the gripper.

The results of the force characterization are shown in Fig. 6. For the push/pull force, the gripper did not make complete rigid contact with the measurement apparatus until after a field strength of around 5 mT, so the data presented in Fig. 6 has been shifted horizontally to only account for loading after the forces became measurable.

The gripper forces should be proportional to the magnetic flux density. Both the gripping force and the push/pull force show approximately linear relationships with respect to the increasing magnetic flux density, as expected. The slope of the best fit lines of the gripping and pushing forces were 0.29 N/T and 0.70 N/T, respectively. The maximum measured gripping

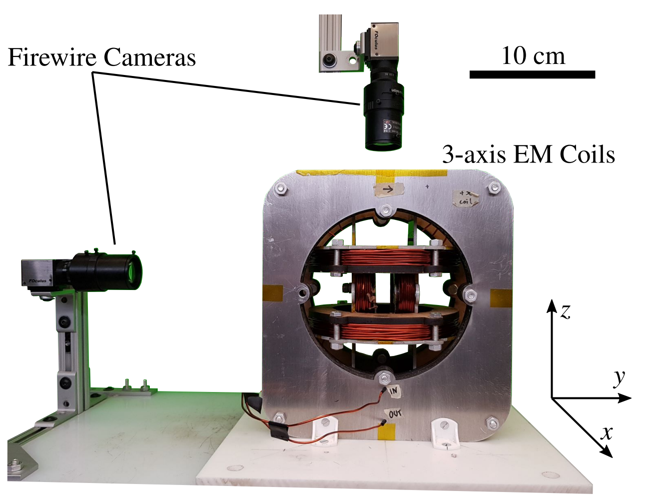

Fig. 4. 3-Axis Helmholtz coil system used for magnetic actuation of the gripper.

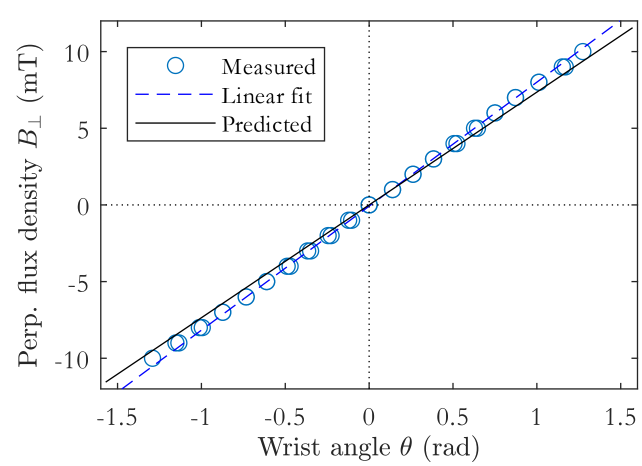

Fig. 5. Applied perpendicular magnetic field $B_\perp$ versus gripper wrist orientation θ.

force was 6 mN and the maximum measured push/pull force was 9 mN.

Experimental clinical-scale magnetic actuation systems have been developed that can accomodate the torso of an adult patient while producing maximum flux densities of 400 mT [14]. Such a system, combined with the gripper prototype presented here, could theoretically produce grip forces of 120 mN and push/pull forces of 180 mN. These forces would exceed the minimum necessary forces for brain tissue retraction of 90 mN per digit tip [15]; therefore, the application of this gripper prototype to minimally-invasive neurosurgical procedures can be considered feasible.

C. Open Loop Performance

This experiment demonstrates the open loop positioning performance of the gripper during a dynamic maneuver.

The open loop control scheme from Section III was used to perform a simple maneuver with the gripper. Fig. 7 shows an example of the gripper wrist position, applied magnetic field components, and absolute position error of the gripper during a constant-jerk maneuver in the horizontal plane. A constant-jerk maneuver was selected to represent the careful motions that a surgeon might perform with the gripper, and it was considered a more accurate representation of the actual use of the device than, for example, a step response, a ramp response, or a sinusoid. Videos of the gripper open loop responses are provided in the supplementary material.

In Fig. 7, the amplitude of the motion is $\pi/4$ rad. The maximum speed, acceleration, and jerk given to the constant-jerk algorithm were $\dot{\gamma}_{max} = 3.14$ rad/s, $\ddot{\gamma}_{max} = 12.22$ rad/s^2, and $\dddot{\gamma}_{max} = 52.36$ rad/s^3, respectively. These values were selected so that the gripper can the maneuver in approximately one second. This speed was considered reasonably fast for a surgical maneuver.

The maximum absolute error during the maneuver was 0.12 rad, or 16% of the amplitude of the maneuver. The error is periodic, and it peaks during the maximum speed sections of the maneuver. The same maneuver was performed at different speeds, and it was found that the error increased with increasing maneuver speed. These observations suggest that the source of the error may be due to the simplifying assumption of the static, rather than dynamic, model used for the gripper wrist.

When performing maneuvers at high speeds or when subjected to a discontinuous loading, significant vibrations occur in the gripper wrist. Due to the elasticity of the compliant wrist and the low damping present in air, these vibrations take tens of seconds to dissipate. The authors consider a settling time greater than 1 s and vibrations during constant-jerk maneuvers greater than 5° to be unsuitable for surgical applications.

Assuming that the system can be represented as a second order, linear time-invariant system, the step response of the system was used to determine the natural frequency and damping ratio. The measured natural frequency of the vibrations was $\omega_n = 64$ rad/s ± 6 rad/s and the 95 % settling time was $t_s \approx 18.7$ s (damping ratio $\zeta_a \approx 0.0025$). The system is significantly underdamped with an overshoot of 75%. These vibrations can only be eliminated with either added sources of damping and friction or through closed-loop control.

For procedures carried out in the ventricles of the brain, it is likely that the device would be operating in a fluidic environment. Cerebrospinal fluid is a Newtonian fluid with a dynamic viscosity of 0.7 to 1.0 mPa·s at 37°C: equally or slightly more viscous than water at the same temperature [16]. The step response of the gripper was recorded while submerged in water. A 95% settling time of $t_s \approx 0.36$ s ($\zeta_w \approx 0.13$) and an overshoot of 42%. In water, the gripper wrist still shows an underdamped response, but the settling time is much more reasonable compared to the settling time in air. In addition, the settling time is a property of the step response, which is not an input profile that would be used

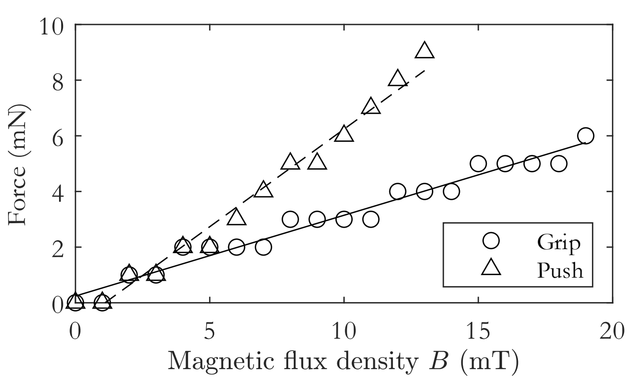

Fig. 6. Measured single-digit gripping force and wrist push/pull force versus applied magnetic flux density (parallel and perpendicular respectively).

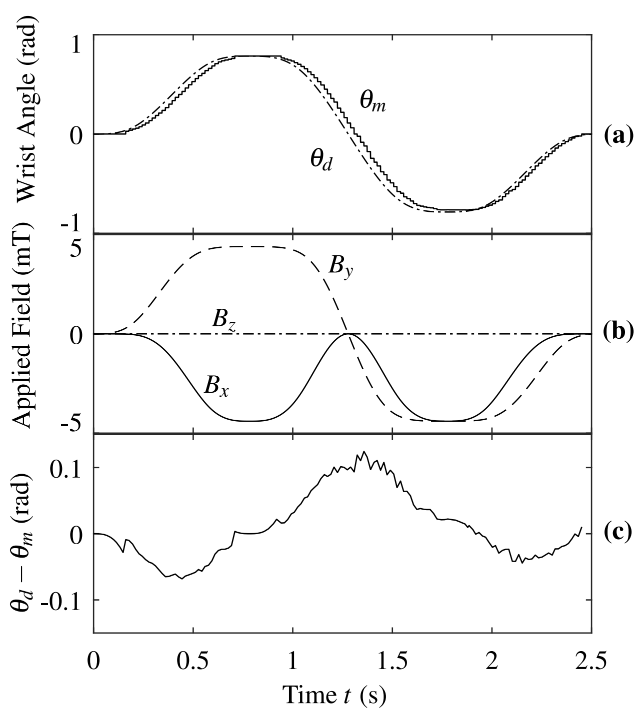

Fig. 7. During an open-loop maneuver: **(a)** Measured and desired wrist angles; **(b)** Applied magnetic field components, **(c)** Error between desired and measured wrist positions.

in practice during surgery. During constant-jerk maneuvers, the vibrations are smaller than the resolution of our vision feedback ($\pm 1°$).

D. Pick-and-Place Demonstration

The purpose of this pick-and-place demonstration is to show that the robot's three degrees of freedom can be controlled independently in practice. The starting location of the cargo was known, and a simple trajectory was planned offline.

The gripper was used to move a 5 mm by 2 mm by 2 mm cargo composed of polydimethylsiloxane (PDMS) in air under open-loop control. The weight of the cargo was 0.2 mN, which would result in a predicted beam deflection of less than 0.2 mm. A video of the pick-and-place demonstration is provided in the supplementary material. Still frames from the video are shown in Fig. 8. The cargo started at an azimuth angle of -0.426 rad. Starting from its resting position (1), the gripper moved above the cargo, grasped (2) and lifted the cargo, transported the cargo (3) to an azimuth angle of $+0.426$ rad, released the cargo (4), then returned to its resting position.

VI. Conclusion

A novel surgical gripper design was presented as a potential method for augmenting existing MIS robots. Wireless magnetic actuation allows a modular high-dexterity tool that could be attached to any type of surgical robot. Open loop control based on a static deflection model was used to control the gripper. Closed loop control may be implemented in the future, but methods of acquiring feedback remains a challenge for all MIS devices. If the device is to be operated in air, closed loop control or a significant redesign will be necessary to mitigate the vibration of the device. Future work for this device will include attaching the device to a positioning robot arm for phantom and ex-vivo trials. Furthermore, increasing the applied forces of the gripper at low field strengths, perhaps via a mechanical transmission, would greatly improve the feasibility of the device.

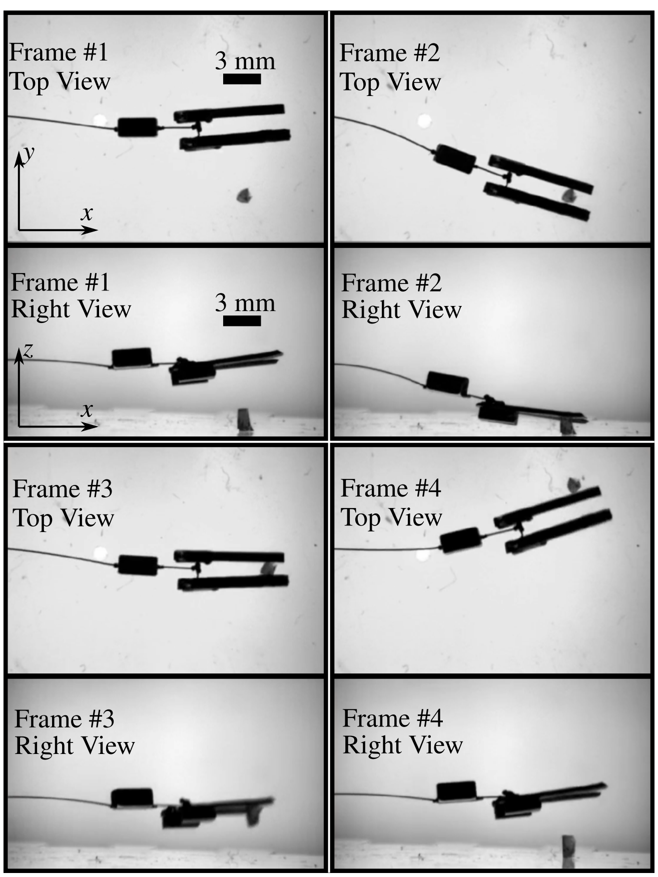

Fig. 8. Still frames from the pick-and-place video. **(1)** Resting position. **(2)** Grasping cargo. **(3)** Moving cargo. **(4)** Releasing cargo.

Acknowledgment

The authors thank Abe Brath for his work assembling and repairing multiple iterations of the prototype gripper.

References

[1] J. J. Doulgeris, S. A. Gonzalez-Blohm, A. K. Filis, T. M. Shea, K. Aghayev, and F. D. Vrionis, "Robotics in Neurosurgery: Evolution, Current Challenges, and Compromises," *Cancer Control*, vol. 22, no. 3, pp. 352–359, July 2015.

[2] G. Guthart and J. Salisbury, "The Intuitive™ Telesurgery System: Overview and Application," in *IEEE Int. Conf. Robot. Autom.*, San Francisco, USA, Apr. 2000, pp. 618–621.

[3] H. J. Marcus, A. Hughes-Hallett, T. P. Cundy, G.-Z. Yang, A. Darzi, and D. Nandi, "da Vinci Robot-Assisted Keyhole Neurosurgery: A Cadaver Study on Feasibility and Safety," *Neurosurg. Rev.*, vol. 38, no. 2, pp. 367–371, Apr. 2015.

[4] G. van Haasteren, S. Levine, and W. Hayes, "Pediatric Robotic Surgery: Early Assessment." *Pediatrics*, vol. 124, no. 6, pp. 1642–9, Dec. 2009.

[5] L. Qiao and M. M. Souweidane, "Purely Endoscopic Removal of Intraventricular Brain Tumors: A Consensus Opinion and Update," *Minim. Invasive Neurosurg.*, vol. 54, no. 04, pp. 149–154, Aug. 2011.

[6] B. G. Rocque, "Neuroendoscopy for Intraventricular Tumor Resection," *World Neurosurg.*, vol. 90, pp. 619–620, June 2016.

[7] N. Simaan, R. M. Yasin, and L. Wang, "Medical Technologies and Challenges of Robot-Assisted Minimally Invasive Intervention and Diagnostics," *Annu. Rev. Control. Robot. Auton. Syst.*, vol. 1, no. 1, pp. 15.1–15.26, May 2018.

[8] M. P. Kummer, J. J. Abbott, B. E. Kratochvil, R. Borer, A. Sengul, and B. J. Nelson, "OctoMag: An Electromagnetic System for 5-DOF Wireless Micromanipulation," *IEEE Trans. Robot.*, vol. 26, no. 6, pp. 1006–1017, Dec. 2010.

[9] J. Zhang, O. Onaizah, K. Middleton, L. You, and E. Diller, "Reliable Grasping of Three-Dimensional Untethered Mobile Magnetic Microgripper for Autonomous Pick-and-Place," *IEEE Robot. Autom. Lett.*, vol. 2, no. 2, pp. 835–840, Apr. 2017.

[10] F. Carpi and C. Pappone, "Stereotaxis Niobe® Magnetic Navigation System for Endocardial Catheter Ablation and Gastrointestinal Capsule Endoscopy," *Expert Rev. Med. Devices*, vol. 6, no. 5, pp. 487–498, Sept. 2009.

[11] A. Z. Taddese, P. R. Slawinski, K. L. Obstein, and P. Valdastri, "Closed Loop Control of a Tethered Magnetic Capsule Endoscope," in *Robot. Sci. Syst.*, Ann Arbor, USA, June 2016.

[12] F. Ullrich, K. S. Dheman, S. Schuerle, and B. J. Nelson, "Magnetically Actuated and Guided Milli-Gripper for Medical Applications," in *IEEE Int. Conf. Robot. Autom.*, Seattle, USA, May 2015, pp. 1751–1756.

[13] S. Salmanipour and E. Diller, "Eight-Degrees-of-Freedom Remote Actuation of Small Magnetic Mechanisms," in *IEEE Int. Conf. Robot. Autom.*, Brisbane, Australia, May 2018, pp. 3608–3613.

[14] J. Rahmer, C. Stehning, and B. Gleich, "Remote Magnetic Actuation Using A Clinical Scale System," *PLoS One*, vol. 13, no. 3, p. e0193546, Mar. 2018.

[15] H. J. Marcus, K. Zareinia, L. S. Gan, F. W. Yang, S. Lama, G.-Z. Yang, and G. R. Sutherland, "Forces Exerted During Microneurosurgery: A Cadaver Study," *Int. J. Med. Robot. Comput. Assist. Surg.*, vol. 10, no. 2, pp. 251–256, June 2014.

[16] I. Bloomfield, I. Johnston, and L. Bilston, "Effects of Proteins, Blood Cells and Glucose on the Viscosity of Cerebrospinal Fluid," *Pediatr. Neurosurg.*, vol. 28, no. 5, pp. 246–251, May 1998.